Electronic Supplementary Material (ESI) for Nanoscale.

Supporting Information

for

Stretching of Immersed Polyelectrolyte Brushes in Shear Flow

Yijun Qiao,[a,b] Qiming He,[a,c] Hsin-Hsiang Huang,[a] Dean Mastropietro,[a] Zhang Jiang,[d] Hua Zhou,[d] Yuhong Liu,[b,*] Matthew V. Tirrell,[a,c*] Wei Chen[a,c*]

[a]Materials Science Division and Center for Molecular Engineering, Argonne National Laboratory, Lemont, Illinois, 60439, USA

[b]State Key Laboratory of Tribology, Tsinghua University, Beijing, 100084, China

[c]X-ray Science Division, Advanced Photon Source, Argonne National Laboratory, Lemont, Illinois, 60439, USA

[*]Corresponding authors: wchen@anl.gov; mtirrell@uchicago.edu; liuyuhong@tsinghua.edu.cn

MOLECULE WEIGHT AND GRAFTING DENSITY

The molecular weight and grafting density of poly(styrene sulfonate) (PSS) brush are evaluated by comparing with a physically adsorbed diblock $PtBS_{20}$-$PSSNa_{420}$ polymer,[1] who has 420 segments of PSSNa (N_1) and a grafting density (σ_1) of 0.0176 chains/nm^2. The thickness of polymer brushes in the osmotic regime is given by $H \sim Nf^{0.5}$, where H is the brush thickness, N is the degree of polymerization, f is the fraction of charged monomers (f = 1 for PSS)[2]. The height of the physically adsorbed PSS brush (H_1) in the osmotic regime was ~100 nm.[1] The height of the PSS brush (H_2) used here was ~190 nm. Thus, the degree of polymerization of the PSS chain used here (N_2) can be evaluated by $N_2 \sim \frac{H_2}{H_1} N_1 \sim 800$, which indicates a molecular weight of around 16,000 g/mol. The mass density of the dry PSS brush is assumed to be 1 g/cm^3. Thus, the two-dimensional mass density of physically adsorbed diblock $PtBS_{20}$-$PSSNa_{420}$ polymer with a dry brush thickness of 1 nm is m_1 = 1 mg/m^2. The two-dimensional mass density of PSS brush used here with an average dry brush thickness of 17 nm is m_2 = 17 mg/m^2. The two-dimensional mass density can also be calculated by $m = A\sigma H$, where A is a constant. Thus, the grafting density of PSS brushes used here is $\sigma_2 = \frac{m_2 H_1}{m_1 H_2} \sigma_1 = 0.15$ chains/nm^2. The degree of polymerization and grafting density of PSS brushes used here are consistent with the results reported by Yu et al.[2,3]

X-RAY REFLECTIVITY OF DRY PSS BRUSHES

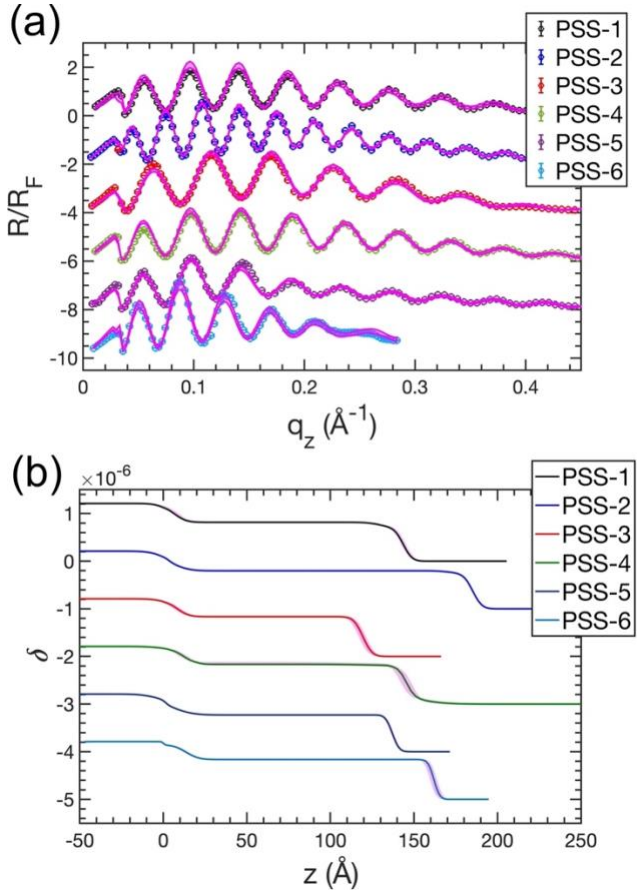

Figure S1. (a) Experimental reflectivity curves (colored circle) and 95% confidence interval (magenta patch) by Hamiltonian MCMC of dry PSS brushes; (b) 95% confidence interval of the δ-profile. The dry PSS brushes 1 – 6 were immersed in water, IPA, and 10 mM nitrate solutions (Cs^+, Ba^{2+}, La^{3+}, and Y^{3+}) to conduct *in situ* shearing measurements, respectively. Thicknesses of dry PSS brushes are in a range from 14 to 20 nm.

TOPOGRAPHY OF PSS BRUSHES

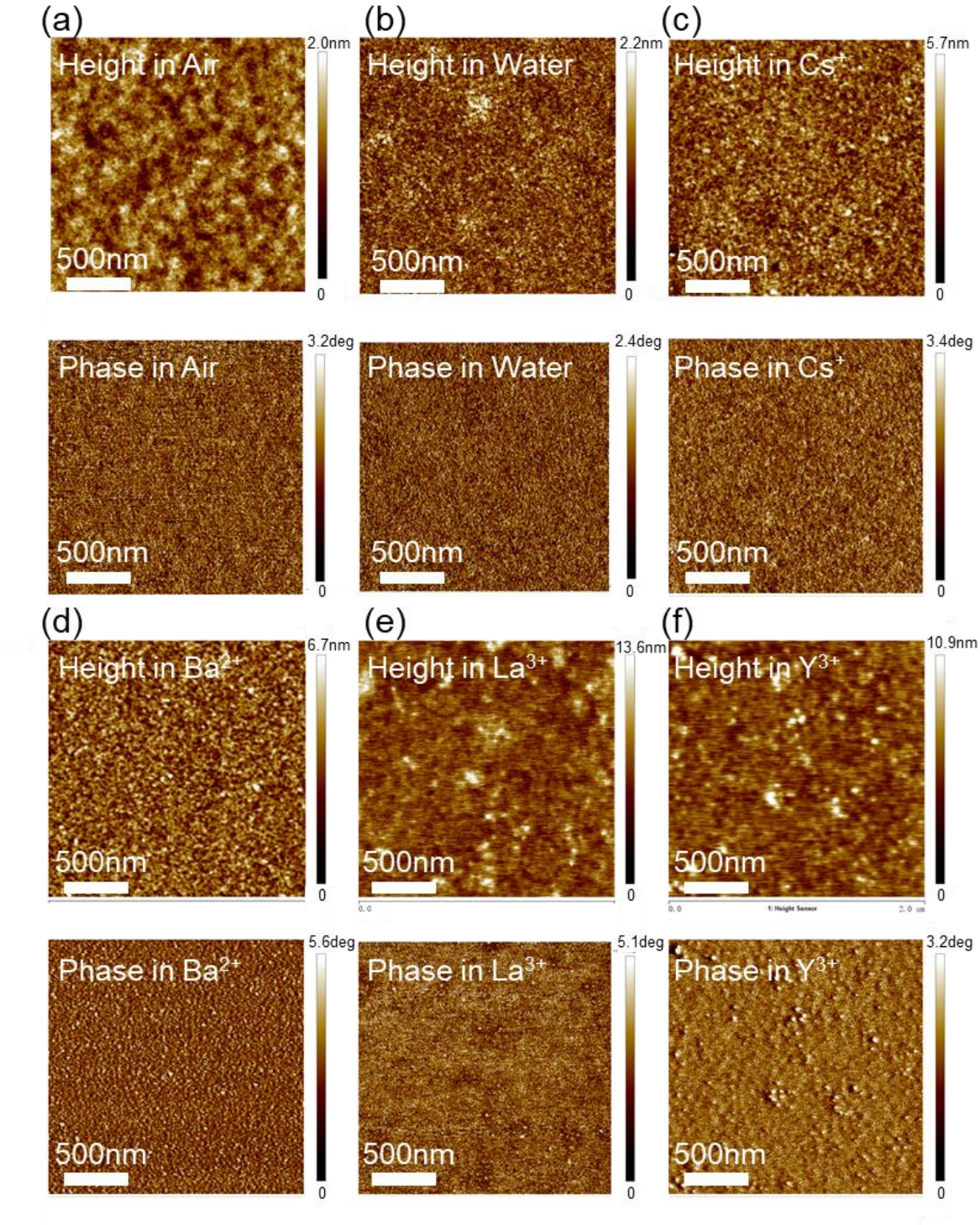

Figure S2. Height and phase topography of PSS brushes measured by atomic force microscopy (Bruker Dimension Icon, USA) with SNL-10 probes and tapping mode: in (a) air; (b) water; (c) $CsNO_3$; (d) $Ba(NO_3)_2$; (e) $La(NO_3)_3$; and (f) $Y(NO_3)_3$ aqueous solutions.

X-RAY REFLECTIVITY OF PSS BRUSHES IN SOLUTION

The 95% confidence interval of the calculated reflectivity obtained from the Hamiltonian MCMC method implies that the layer model well describes the reflectivity and gives a reasonable estimation for the δ profile of PSS brushes in solution. An initial δ value and physical boundaries are needed in the model prediction process. For PSS brushes or films, the mass density reported by the previous literatures[4–10] is in a range of 1.0 ~ 1.5 g/cm^3 and the corresponding calculated δ is in a range of 5.34 ~ 8.02×10^{-7} under an X-ray wavelength of 0.62 Å (20 keV). An upper δ boundary of 1×10^{-5} and a lower δ boundary of 1 × 10^{-7} for PSS brushes are applied. Pure constituents include IPA, H_2O, $CsNO_3$, $Ba(NO_3)_2$, $La(NO_3)_3$, $Y(NO_3)_3$ are also used in the XRR. The mass density of the pure constituents and the calculated δ are shown in the following Table S1. The measured mass density of the 10 mM $CsNO_3$, $Ba(NO_3)_2$, $La(NO_3)_3$ and $Y(NO_3)_3$) aqueous solutions and the calculated δ are shown in Table S2, which were used in the model fitting to determine the initial δ of the buffer layer.

Table S1. The mass density and calculated δ of the used pure constituents

Pure constituents	PSS	IPA	water	$CsNO_3$	$Ba(NO_3)_2$	$La(NO_3)_3$	$Y(NO_3)_3$
Mass density (g/cm^3)	1.0 – 1.5[4–10]	0.7845	0.9972	3.68	3.24	1.3	2.682
Calculated δ (×10^{-7})	5.34 – 8.02[4–10]	4.61	5.75	16.77	15.14	6.22	13.29

Table S2. The measured mass density by a density meter (Anton Paar Density Meter DMA 35, Austrian) and calculated δ of 10 mM salt solutions

Nitrate solution	$CsNO_3/H_2O$	$Ba(NO_3)_2/H_2O$	$La(NO_3)_3/H_2O$	$Y(NO_3)_3/H_2O$
mass density (g/cm^3)	0.9987	0.9995	1.0001	0.9996
calculated δ (×10^{-7})	5.757	5.762	5.765	5.763

Note: The parameters for modeling the layers (thickness and X-ray refractive index) and interfaces (standard deviation and asymmetry factor) do not necessarily represent physical parameters by themselves. Instead, they should be interpreted together as latent variables for constructing a continuous smooth profile, a similar concept to that in the curve decomposition with basis functions.

Table S3. The mean of the model parameters of PSS brush in IPA estimated with a two-layer model by Hamiltonian MCMC and their standard deviations

Shear rate / s^{-1}	Layer	Thickness / Å	Dispersion δ / $\times 10^{-7}$	Roughness / Å
0	1	20.6 (0.9)	4.97 (0.02)	15.9 (1.0)
	2	166.1 (0.2)	8.11 (0.01)	9.4 (0.1)
30	1	9.9 (1.6)	4.90 (0.15)	11.1 (1.3
	2	176.4 (0.5)	7.69 (0.05)	7.9 (0.4)
150	1	17.5 (1.6)	4.99 (0.04)	15.6 (0.9)
	2	183.9 (0.2)	7.71 (0.01)	8.2 (0.2)
300	1	20.5 (2.0)	4.72 (0.04)	12.1 (1.5)
	2	184.5 (0.3)	7.65 (0.01)	9.7 (0.1)
750	1	18.6 (1.6)	5.52 (0.03)	22.4 (0.7)
	2	184.0 (0.1)	7.79 (0.01)	7.3 (0.2)

Table S4. The mean of the estimated model parameters of PSS brush in water with a one-layer model by Hamiltonian MCMC and their standard deviations

Shear rate / s^{-1}	Thickness / Å	Dispersion δ / $\times 10^{-7}$	Roughness / Å
0	1005.4 (62.5)	7.43 (0.01)	371.6 (5.1)
30	932.1 (130.3)	7.26 (0.04)	362.5 (11.2)
150	1273.3 (22.5)	7.32 (0.02)	367.7 (8.5)
300	1448.9 (32.8)	7.26 (0.02)	358.7 (9.3)
750	1540.0 (43.4)	7.24 (0.02)	317.3 (11.7)

Table S5. The mean of the estimated model parameters of PSS brush in $CsNO_3$ solution estimated with a one-layer model by Hamiltonian MCMC and their standard deviations

Shear rate / (s^{-1})	Thickness / Å	Dispersion δ / $\times 10^{-7}$	Roughness / Å
0	1259.7 (52.9)	7.52 (0.02)	378.8 (3.8)
30	929.0 (198.7)	7.51 (0.03)	391.5 (3.0)
75	925.2 (172.9)	7.54 (0.03)	370.4 (4.7)
150	864.2 (118.5)	7.53 (0.03)	408.3 (2.9)
300	1226.0 (118.6)	7.60 (0.02)	384.4 (2.5)
525	773.1 (209.9)	7.33 (0.03)	381.2 (3.1)
750	1966.2 (53.3)	7.02 (0.02)	363.9 (2.7)

Table S6. The mean of the estimated model parameters of PSS brush in $Ba(NO_3)_2$ solution estimated with a three-layer model by Hamiltonian MCMC and their standard deviations

Shear rate / s^{-1}	Layer	Thickness / Å	Dispersion δ / $\times 10^{-7}$	Roughness / Å
0	1	78.2 (5.1)	12.2 (0.3)	76.8 (3.9)
	2	9.4 (0.5)	11.3 (0.4)	28.3 (2.8)
	3	10.5 (0.4)	8.4 (0.1)	6.3 (0.4)
75	1	95.6 (1.0)	11.2 (0.3)	77.5 (4.1)
	2	9.7 (0.3)	10.0 (0.2)	29.0 (1.4)
	3	11.5 (0.4)	8.28 (0.08)	6.7 (0.2)
150	1	91.7 (2.0)	12.4 (0.1)	97.6 (3.4)
	2	7.7 (1.5)	11.0 (0.1)	25.2 (1.9)
	3	10.6 (0.5)	8.84 (0.09)	6.7 (0.2)
300	1	97.5 (1.3)	11.4 (0.2)	80.0 (4.8)
	2	11.7 (0.8)	10.3 (0.2)	29.3 (1.8)
	3	11.7 (0.3)	8.45 (0.08)	7.1 (0.3)
750	1	99.0 (1.8)	12.3 (0.1)	96.7 (5.1)
	2	9.4 (0.6)	10.9 (0.1)	25.8 (2.0)
	3	11.5 (0.4)	8.69 (0.07)	6.2 (0.3)
1050	1	94.6 (2.2)	12.4 (0.1)	90.3 (4.8)
	2	9.8 (1.2)	11.3 (0.1)	24.1 (1.7)
	3	10.8 (0.5)	8.8 (0.1)	6.6 (0.3)
1350	1	98.2 (3.1)	12.5 (0.1)	79.5 (5.5)
	2	11.3 (0.3)	11.3 (0.1)	25.6 (2.9)
	3	10.3 (0.4)	8.63 (0.08)	7.4 (0.3)
1500	1	102.3 (1.9)	12.4 (0.1)	84.0 (2.7)
	2	10.5 (0.3)	11.1 (0.1)	26.1 (1.8)
	3	11.3 (0.3)	8.64 (0.06)	6.5 (0.2)

Table S7. The mean of the estimated model parameters of PSS brush in $La(NO_3)_3$ solution estimated with a four-layer model by Hamiltonian MCMC and their standard deviations

Shear rate / s^{-1}	Layer	Thickness / Å	Dispersion δ / $\times 10^{-7}$	Roughness / Å
0	1	65.6 (0.1)	8.31 (0.04)	104.9 (0.2)
	2	21.7 (0.1)	8.41 (0.03)	1.0 (0.1)
	3	13.3 (0.1)	7.79 (0.02)	2.6 (0.1)
	4	2.9 (0.1)	9.73 (0.03)	6.5 (0.1)
75	1	67.0 (0.1)	8.40 (0.02)	109.8 (0.2)
	2	21.4 (0.1)	8.50 (0.02)	1.0 (0.1)
	3	11.9 (0.1)	8.02 (0.08)	2.9 (0.1)
	4	2.4 (0.1)	9.28 (0.02)	6.0 (0.1)
150	1	68.0 (0.9)	8.18 (0.09)	106.3 (1.4)
	2	19.4 (0.2)	8.27 (0.08)	1.1 (0.1)
	3	13.0 (0.1)	7.83 (0.06)	2.2 (0.1)
	4	2.3 (0.1)	9.10 (0.07)	6.2 (0.1)
300	1	71.7 (5.7)	7.96 (0.02)	114.8 (7.6)
	2	23.6 (4.7)	8.07 (0.01)	1.1 (0.1)
	3	12.1 (1.4)	7.49 (0.02)	3.0 (0.4)
	4	2.1 (0.3)	9.87 (0.05)	5.5 (0.7)
750	1	85.5 (2.7)	8.07 (0.08)	108.0 (3.9)
	2	26.5 (0.8)	8.02 (0.07)	1.1 (0.1)
	3	12.0 (0.3)	7.55 (0.08)	2.7 (0.1)
	4	1.9 (0.1)	8.96 (0.02)	4.4 (0.2)

Table S8. The mean fitting parameter and the standard deviation (SE) of the PSS brush in $Y(NO_3)_3$ fitted with a three-brush-layer model

Shear rate / s^{-1}	Layer	Thickness / Å	Dispersion δ / $\times 10^{-7}$	Roughness / Å
0	1	120.8 (6.6)	6.56 (0.03)	24.9 (1.8)
	2	86.4 (6.3)	7.38 (0.13)	98.6 (3.5)
	3	69.1 (1.6)	5.76 (0.01)	26.4 (1.6)
75	1	103.7 (3.4)	6.93 (0.06)	32.3 (1.6)
	2	99.5 (3.7)	7.21 (0.08)	104.0 (4.9)
	3	72.8 (1.4)	5.78 (0.01)	22.7 (0.8)
150	1	126.3 (4.7)	6.59 (0.08)	29.0 (1.4)
	2	84.6 (4.6)	7.26 (0.05)	99.8 (3.3)
	3	68.7 (0.8)	5.76 (0.01)	24.7 (0.8)
300	1	96.2 (11.7)	6.61 (0.09)	27.5 (3.6)
	2	116.0 (15.1)	7.50 (0.23)	117.1 (12.3)
	3	70.4 (1.2)	5.76 (0.01)	25.4 (2.1)
750	1	84.8 (7.4)	6.41 (0.09)	23.2 (2.5)
	2	139.3 (10.4)	7.09 (0.05)	132.8 (7.7)
	3	66.3 (0.8)	5.83 (0.06)	22.1 (0.9)

Statistical Significance

It is important to note that the observed shear-induced changes, as evident from the X-ray reflectivity (XRR) fringes, go beyond the range of experimental errors. The lines and arrows are added in the Zoom-In plots of Figure 5 - 7 (Figure S3) as visual guidance to indicate the changes in XRR fringes. To capture these changes, we conducted a rigorous analysis of the XRR data by employing the effective density model with the Hamiltonian Markov Chain Monte Carlo (MCMC) method, which is well-recognized for its statistical robustness.

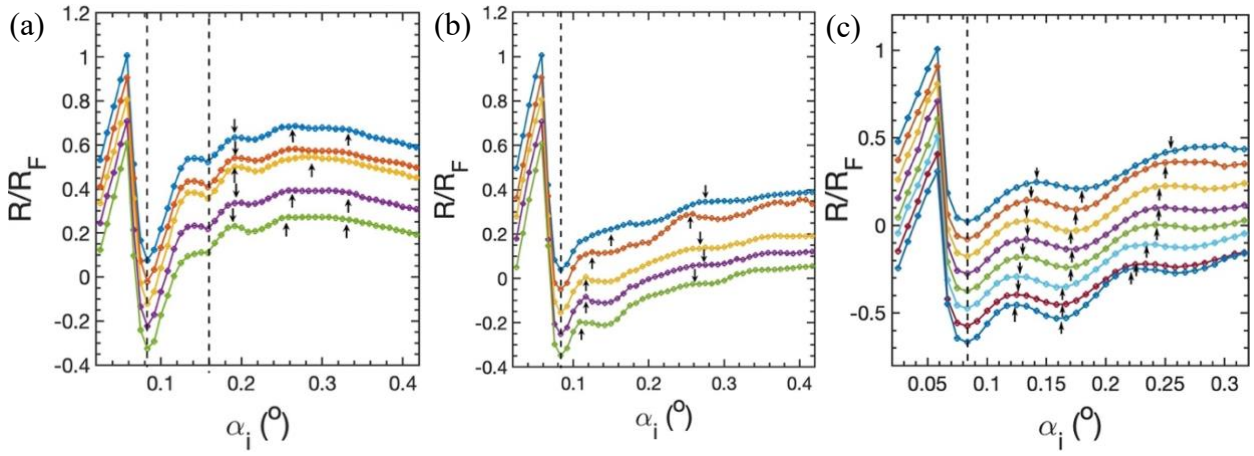

Figure S3. Zoomed-In plots showing shear-induced changes in XRR raw data ((a) – (c) correspond to figures 5 – 7 in the manuscript).

Hamiltonian MCMC, with appropriate preconditioning, is known for its superior performance compared to random walk MCMC methods. It is an efficient tool for the statistical analysis of parameter distributions, model predictions, and confidence intervals. In our Hamiltonian MCMC analysis, we employed the No-U-Turn Sampler to generate 5000 draws from the target posterior distribution. These draws served multiple purposes, including predictive modeling and the computation of confidence intervals. The 95% confidence intervals for both reflectivity and the Electron Density Profile (EDP) were calculated based on post-burn-in iterations and prominently featured as pink-shaded regions in the respective figures. To facilitate a clearer understanding of the observed changes, arrows were thoughtfully added to the Zoom-In plots in Figures 3 and 4, serving as visual indicators of these variations.

Notably, the discernible shifts in the pink-shaded regions (Figure S4) within these figures suggest changes that extend beyond the range of error bars, which represent standard deviations derived from our Hamiltonian MCMC analysis. While it's true that some changes at specific shear rates overlap with the error bars, it is essential to recognize that the relative trends we observed hold significant statistical significance.

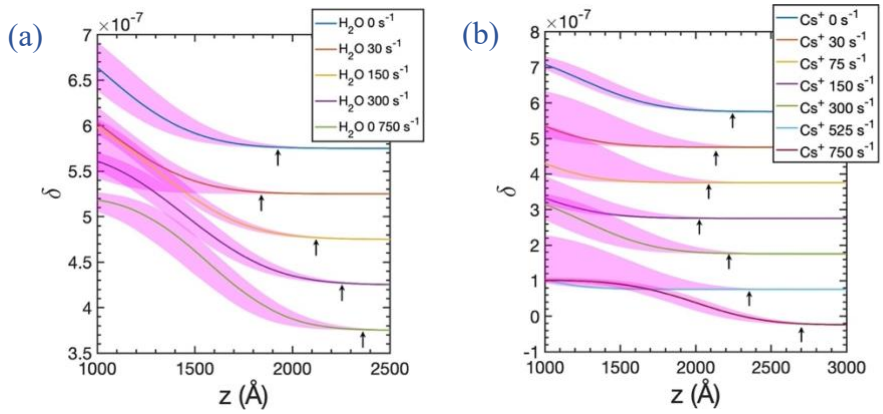

Figure S4. Zoomed-In plots showing shear-induced changes in EDP profiles ((a) and (b) correspond to figures 3 and 4 in the manuscript).

SOLUTION PROPERTY

Table S9. Measured pH value of solvents (water, IPA, and 10 mM $CsNO_3$, $Ba(NO_3)_2$, $La(NO_3)_3$, $Y(NO_3)_3$ aqueous solutions) by a pH meter (Mettler Toledo FiveEasy™ Plus pH, Switzerland).

Parameter	Water	IPA	$CsNO_3$	$Ba(NO_3)_2$	$La(NO_3)_3$	$Y(NO_3)_3$
pH	6.30	5.75	4.86	5.31	4.88	4.78

THE RELATIONSHIP BETWEEN NEUTRON REFLECTIVITY AND X-RAY REFLECTIVITY EXPERIMENTS

The experimental conditions in the previously conducted Neutron Reflectivity studies differ from our X-ray reflectivity approach. Baker[11,12] and Nguyen[13] et al. found that flow shear had no impact on the thickness of neutral polystyrene brushes using Neutron Reflectivity. Notably, there are three key distinctions between their experiments and our own.

Firstly, the cited studies employed copolymers of neutral polystyrene brushes, while our research centered on negatively charged PSS brushes. The presence of interchain electrostatic interactions and the interaction of PSS brushes with water yields a distinct structural response to shear flow compared to neutral polymer brushes.

Secondly, their studies utilized a fluid cell with plane Poiseuille flow, focusing on high shear rates exceeding 104 s^{-1}. In contrast, our work employed a cone-plate geometry encompassing both tangential Couette flow and vertical upward flow, encompassing shear rates spanning from 0 to 1500 s^{-1}.

Thirdly, the Neutron Reflectivity studies relied on small q ranges of 0 – 0.06 $Å^{-1}$ or 0 – 0.1 $Å^{-1}$, whereas our XRR approach encompassed a broader q range of 0 – 0.5 $Å^{-1}$.

The outcomes of the previous Neutron Reflectivity investigations lend support to our X-ray reflectivity findings. Gutfreund et al.[14] established that polymer brush chains experience shrinkage under weak shears below 30 s^{-1}, as evidenced by neutron reflectivity. Although Gutfreund's experiments involved polystyrene brushes immersed in entangled polymer solutions, their findings still provide insights applicable to our work. They noted that a steady shear flow could induce a horizontal shift of the center of mass, leading to chain tilting and thickness reduction. This principle holds true for grafted polymer brushes immersed not only in polymer solutions but also in solvents. Moreover, Gutfreund's work concluded that the nonlinear thickness reduction of polystyrene brushes resulted from the normal stress exerted by free polymer chains in the solution. This aligns with our findings, as the extra shear stress perpendicular to the applied shear flow emerges as a pivotal factor in determining the shear response of polymer brushes—mirroring our own results.

In the context of our cone-plate geometry, the additional upward shear flow induced by centrifugal force plays a vital role. This force generates a radial velocity component, leading to outward flow near the cone wall. Through the conservation of mass and fluid continuity, an inward flow occurs at the stationary substrate's surface, while an upward flow manifests within the geometry's gap. The shear stress exerted by this upward flow triggers the stretching of our PSS brushes and an ensuing increase in brush thickness.

REFERENCE

1 R. Farina, N. Laugel, J. Yu and M. Tirrell, *J. Phys. Chem. C*, 2015, **119**, 14805–14814.

2 J. Yu, N. E. Jackson, X. Xu, Y. Morgenstern, Y. Kaufman, M. Ruths, J. J. De Pablo and M. Tirrell, *Science*, 2018, **360**, 1434–1438.

3 J. Yu, J. Mao, G. Yuan, S. Satija, Z. Jiang, W. Chen and M. Tirrell, *Macromolecules*, 2016, **49**, 5609–5617.

4 C. M. Miyazaki, M. Maria, D. D. Borges, C. F. Woellner and J. A. Riul, 2017, **1705**, 10673.

5 Y. Lvov, K. Ariga, I. Ichinose and T. Kunitake, *J. Am. Chem. Soc.*, 1995, **117**, 6117–6123.

6 J. B. Schenkman, I. Jansson, Y. Lvov, J. F. Rusling, S. Boussaad and N. J. Tao, *Arch. Biochem. Biophys.*, 2001, **385**, 78–87.

7 T. Cui, Y. Lvov, J. Shi and H. Feng, *Encycl. Nanosci. Nanotechnol.*

8 M. Antonietti, J. Conrad and A. Thuenemann, *Macromolecules*, 1994, **27**, 6007–6011.

9 L. A. Prezyna, G. E. Wnek, Y.-J. QIU and J. R. Reynolds, *Synth. Met.*, 1991, **41**, 979–981.

10 P. Kaewsaiha, K. Matsumoto and H. Matsuoka, *Langmuir*, 2004, **20**, 6754–6761.

11 S. M. Baker, A. Callahan, G. Smith, C. Toprakcioglu and A. Vradis, *Phys. B Condens. Matter*, 1997, **241**, 1041–1047.

12 S. M. Baker, G. S. Smith, D. L. Anastassopoulos, C. Toprakcioglu, A. A. Vradis and D. G. Bucknall, *Macromolecules*, 2000, **33**, 1120–1122.

13 D. Nguyen, C. J. Clarke, A. Eisenberg, M. H. Rafailovich, J. Sokolov and G. S. Smith, *J. Appl. Crystallogr.*, 1997, **30**, 680–683.

14 A. Korolkovas, C. Rodriguez-Emmenegger, A. de los Santos Pereira, A. Chenneviere, F. Restagno, M. Wolff, F. A. Adlmann, A. J. Dennison and P. Gutfreund, *Macromolecules*, 2017, **50**, 1215–1224.